Signature Analysis of Multifrequency Polarimetric Nasa DC-8 Airsar Data of Alpine Geo-Applications

K.P. Papathanassiou and M.F. Buchroithner

Institute for Image Processing and Computer Graphics,
Joanneum Research, Graz, Austria

ABSTRACT

In this paper several techniques to analyze multifrequency polarimetric radar data acquired by the NASA/JPL airborne SAR for alpine geo-applications are described. Specifically, procedures for the determination of the heterogeneity of scatterers and of the polarization purity of the return signal, the generation of images optimizing the return signal of different surface cover types, and the enhancement of the contrast between different surface categories are presented.

INTRODUCTION

An imaging radar polarimeter is an instrument that permits measurements of the full polarization information for each resolution element. This is achieved by employing two orthogonally polarized antennas and recording both amplitude and absolute phase of the received electric field transversally (Zebker, van Zyl and Held 1987). The full polarization information is contained in a mathematical formulation called the scattering matrix.

The final goal of the present study is to provide the physical basic for the thematic mapping of high-alpine environments. However the investigations set forth in this paper represent only a first step. The image data cover the well-known Oetztal testsite in the Central Alps of Tyrol (Austria). Figure 1 gives an overview of the northeastern part of the study area. It has been surveyed by the three-frequency polarimetric AIRSAR of the Jet Propulsion Laboratory (JPL) on board of the NASA DC-8 on 18 August 1989.

In particular, techniques are described for: 1) the determination of the heterogeneity of scatterers; 2) the determination of the polarization purity of the return signal; 3) the generation of images that optimize the return signal of different surface cover types; and 4) the performance of a contrast enhancement between different surface categories.

Fig. 1 - Overview of the northeastern part of the Oetztal testsite showing the Hintereis Glacier and the glaciated peak of Weisskugel (3768 m). The rocky ridges, moraines (left and foreground), and the slopes covered by alpine meadows were taken as sample sites. Alpine forest can only be found further down the valley.

1. BASIC CONSIDERATIONS

At each point in space the electric field vector of a plane monochromatic wave rotates in a plane perpendicular to the direction of propagation and in doing so traces out an ellipse, the polarization ellipse. The shape of this ellipse is completely described by two geometrical parameters, the ellipticity angle χ and the ellipse orientation angle ψ. The handedness of the polarization is indicated by the sign of the ellipticity angle. Negative values of χ indicate right-handed, positive values left-handed polarization. A linear polarization is indicated by $\chi = 0°$, circular polarization by $\chi = 45°$. Also notice that values of χ vary between 45° and 45°.

The polarization state of a plane wave can be alternatively characterized by the four Stokes parameters

I_0, Q, U and V. The Stokes parameters can be written in vector form as follows:

$$\vec{S} = \begin{pmatrix} I_0 \\ Q \\ U \\ V \end{pmatrix} = \begin{pmatrix} S_0 \\ S_1 \\ S_2 \\ S_3 \end{pmatrix} = \begin{pmatrix} I_0 \\ I_0 \cos 2\chi \cos 2\psi \\ I_0 \cos 2\chi \, sen\, 2\psi \\ I_0 \sin 2\chi \end{pmatrix} \quad (1)$$

We refer to the above representation as the Stokes vector for a completely polarized wave. I_0 is propotional to the total intensity of the wave.

The scattering behavior of an object can be modelled by a complex 2x2 scattering matrix. The scattering matrix describes how the scatterer transforms the illuminating wave. In other words it relates the electric field components of the scattered and illuminating waves:

$$\begin{pmatrix} E_h^{sc} \\ E_v^{sc} \end{pmatrix} = \frac{\exp(ikr)}{kr} \begin{pmatrix} S_{11} S_{12} \\ S_{21} S_{22} \end{pmatrix} \begin{pmatrix} E_h^{ill} \\ E_v^{ill} \end{pmatrix} \quad (2)$$

where: E_h^{sc}, E_v^{sc} and E_h^{ill}, E_v^{ill} are the horizontally and vertically polarized components in the scattered and illuminating wave, S_{ij} are the components of the scattering matrix (also know as the complex scattering amplitudes), r is the distance between the scatterer and the receiving antenna, and k is the wave number of the illuminating wave.

Each element of the scattering matrix is a function of frequency and scattering and illumination angles. In the case of monostatic radar geometry it is symmetrical and contains only up to five independent quantities: three amplitudes and two relative phases.

Analogically to the 2x2 complex scattering matrix is the 4x4 real Stokes (reflection) matrix (Boerner et al. 1992). This matrix relates the Stokes parameters of the scattered wave S_i^{sc} to the Stokes parameters of the illuminating wave S_j^{ill}. The scatterer can thus be characterized in terms of the Stokes matrix [M] where:

$$\begin{pmatrix} S_0 \\ S_1 \\ S_2 \\ S_3 \end{pmatrix}^{sc} = [R][M][R] \begin{pmatrix} S_0 \\ S_1 \\ S_2 \\ S_3 \end{pmatrix}^{ill} \quad (3)$$

[R] is a given 4x4 matrix.

The elements of [M] are functions of the elements of the scattering matrix. In the monostatic case, [M] is a symmetric matrix. The average Stokes parameters of the waves scattered by an object that vary statistically, either in time or in space, are related to the Stokes parameters of the illuminating wave through an average Stokes matrix which can be calculated by averaging the elements of [M].

Knowledge of the scattering matrix for a polarization state permits, through suitable transformations (Ulaby, Elachi and editors 1990), to calculate the matrix corresponding to any state of polarization. In other words, from the measured scattering matrix it is possible to calculate the received power for any possible combination of transmitting and receiving antennas. This process is called polarization synthesis.

The power received by an antenna, whose polarization is characterized by the Stokes vector $\vec{S}_{rec}$ is given by:

$$P = K(\lambda, \theta, \phi) \begin{pmatrix} S0 \\ S1 \\ S2 \\ S3 \end{pmatrix}^{sc} [M] \begin{pmatrix} S0 \\ S1 \\ S2 \\ S3 \end{pmatrix}^{ill} \quad (4)$$

where $\vec{S}_{tr}$ is the Stokes vector of the transmitting antenna and K is given by:

$$K(\lambda, \theta, \phi) = \sqrt{\frac{\varepsilon_0}{\mu_0}} = \frac{g(\theta, \phi)}{E^2} \quad (5)$$

and $g(\theta, \phi)$ is the antenna gain function.

The individual power measurements for each radar resolution element are only related statistically. Therefore several power measurements are added to reduce statistical variation, but at the expence of a loss in spatial resolution. The total power received from a set of N measurements can be expressed by:

$$p^{rec} = \sum_{i=1}^{N} P_i^{rec} \quad (6)$$

where P_i^{rec} is the power received from the i-th individual measurement. Thus the same antennas are used for each observation and the factor K is assumed to be constant over the averaging interval.

$$P^{rec} = K(\lambda, \phi) \begin{pmatrix} S_0 \\ S_1 \\ S_2 \\ S_3 \end{pmatrix}^{rec} \left(\sum_{i=1}^{N} [M]_i \right) \begin{pmatrix} S_0 \\ S_1 \\ S_2 \\ S_3 \end{pmatrix}^{tr} \quad (7)$$

Here is $[M]_i$ the Stokes matrix of the i-th measurement.

A particular graphic presentation of the variation of the received power as a function of the polarization of the transmitted wave, known as the polarization signature, is quite useful to describe polarization properties of point and distributed targets (van Zyl, Zebker and Elachi, 1987).

The signatures are shown in the form of plots of synthesized power as a function of ellipticity and orientation angles of the transmitting wave.

2. DATA ANALYSIS

As initially mentioned, the final purpose of the methods developed is the thematic mapping of high alpine environments with SAR image data. This is based on several data analysis steps that have been developed for the use of radar polarimetry in earth science investigations.

The SAR data cover an image swath of 10 x 12 km^2. The system operated at three frequency bands: P-band (440 MHz), L-band (1.25 GHz) and C-band (5.30 GHz). The flying height was approx. 8200 m above sea level. The data were processed at JPL and delivered in a 4-looks compressed data format (Dubois and Norikane 1987) with a pixel size of 12.2 m (azimuth) x 6.66 m (range). Calibration was performed by the Radar Group of the Institute for Meteorology and Geophysics of the University of Innsbruck. Figure 2 shows a geocoded Landsat TM, Figure 3 a geocoded AIRSAR image of the testsite.

The selected surface cover which the investigations are based on are bare rock (3x3 pixel), moraines (5x5 pixel), alpine meadows (3x3 pixel) and alpine spruce forest (3x3 pixel). Considering the geometric depedence of the signatures on their terrain position, only characteristic ones for each surface class will be presented. The locations of the test areas from which these representative signatures were derived are indicated in Figure 3.

2.1 Co- and cross-polarized signatures

Since the complete receive and transmit antenna configuration is described by a four-dimensional space, only a two dimensional space is represented, fixing the receive

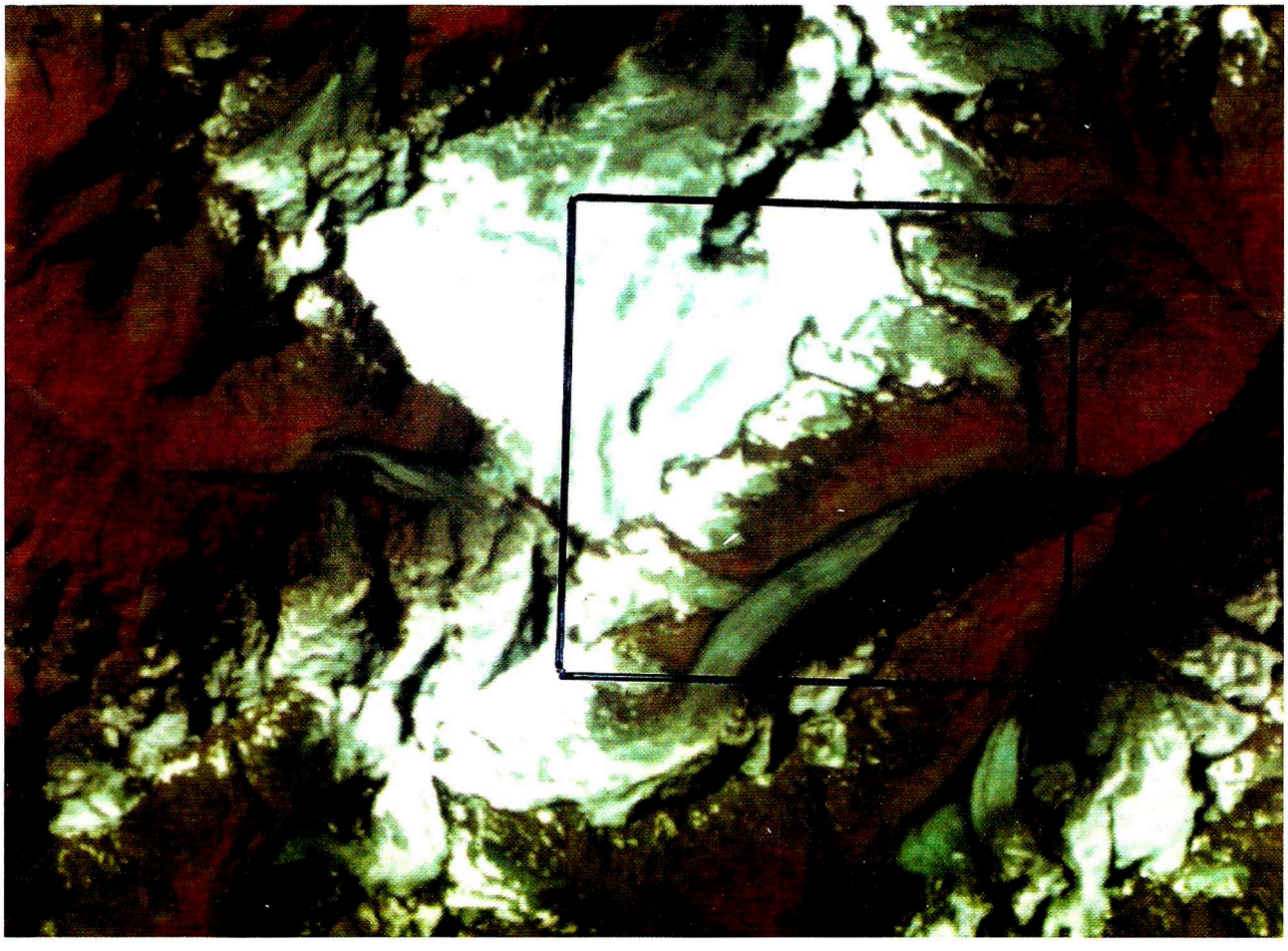

Fig. 2 - Landsat-TM scene of testsite with bands 4, 3 and 2 in red, green and blue. Valley in the lower right quarter is the Upper Vent Valley.

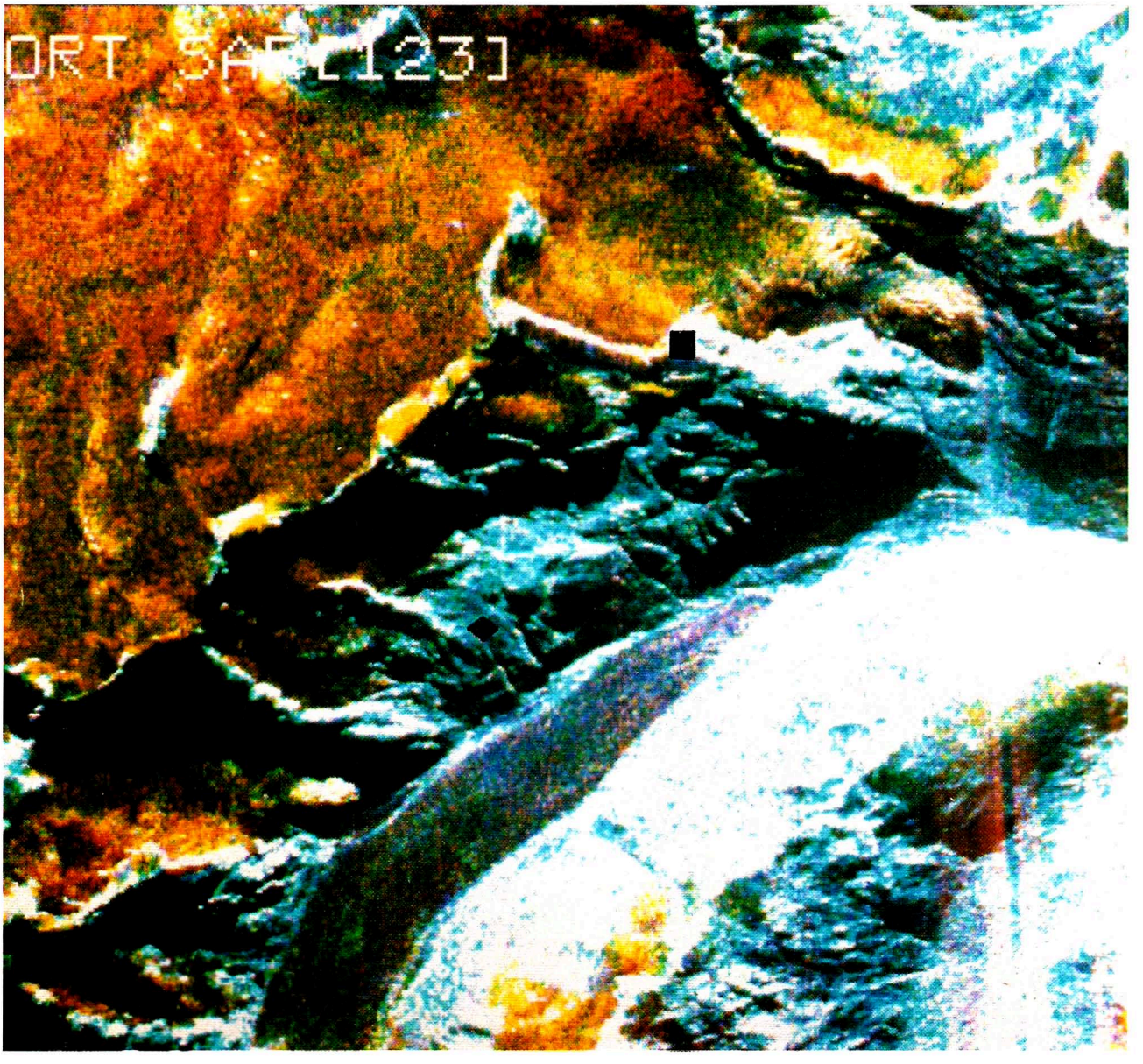

Fig. 3 - Geocoded AIRSAR image of the subarea framed in Figure 2. RGB composite of P, L and C-band showing test areas for rock indicated with ❐, moraines indicated with ◊ and alpine meadows indicated with Δ.

antenna configuration at the same ellipticity and at two orientations: in the case of co-polarization a like orientation, in the case of cross-polarization an orthogonal orientation. In both cases, the synthesized power is plotted as a function of the transmitting antenna polarization. Figures 4 and 5 show the co- and cross-polarized signatures of the selected surface categories (A.P.Agrawal and W-M. Boerner 1991). We can see that the signature shapes from the same surface class are not identical in the different frequency bands and this is because the signal reflectances are dispersive (function of the frequency), and as a consequence also the received power. The received power is also a function of the radar illumination angle, with the consequence that signatures from the same surface class in different terrain positions (with a different illumination angle) have no identical but only similar shapes.

This problem is significant for alpine environments. However, to some extent by means of a Fourier analysis (Reck and Shreier 1990) the drawbacks generated through this very great similarity might be overcome.

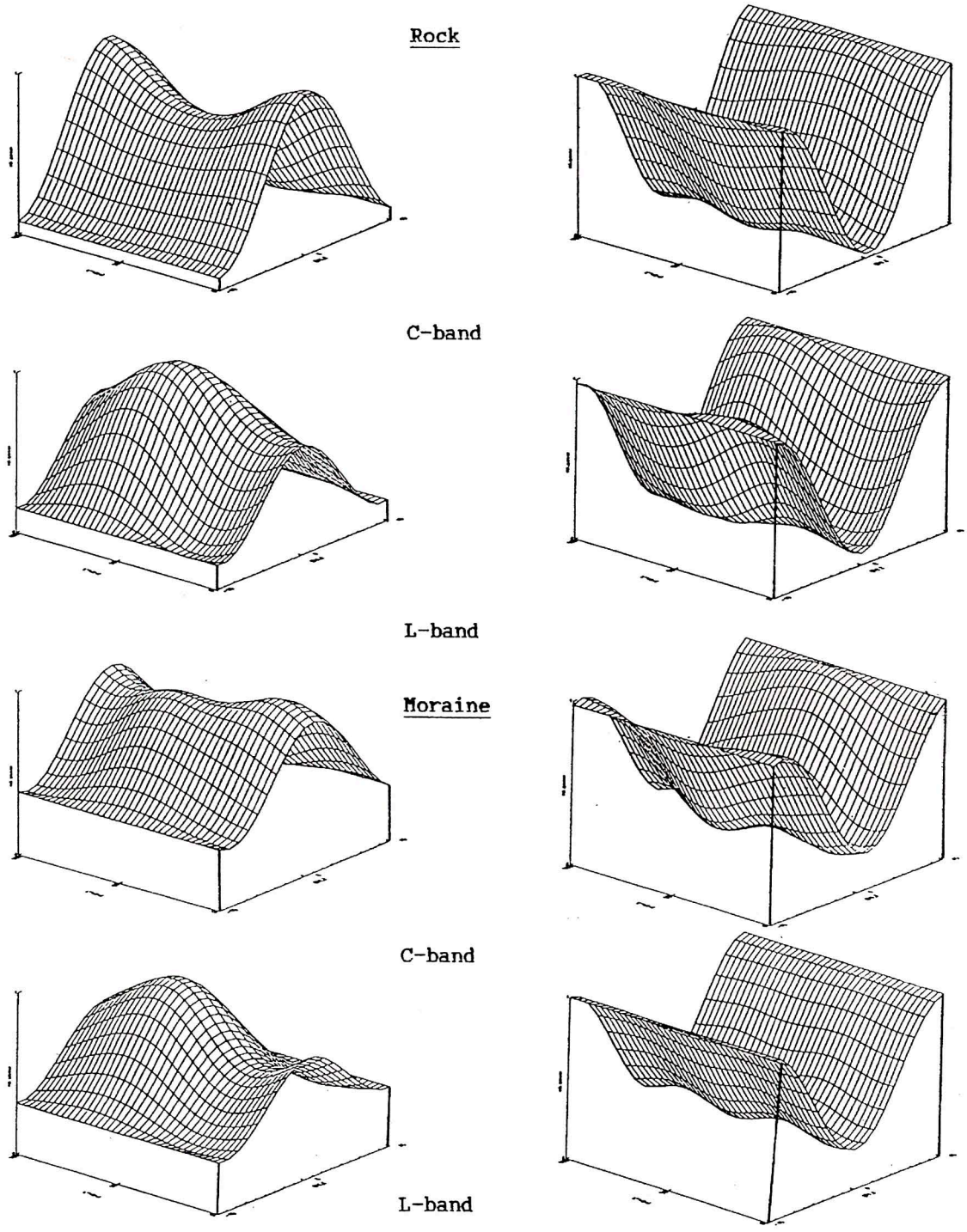

Fig. 4 - Polarization signatures (left: co-polarized, right: cross-polarized) of bare rock and moraine of C- and L-band.

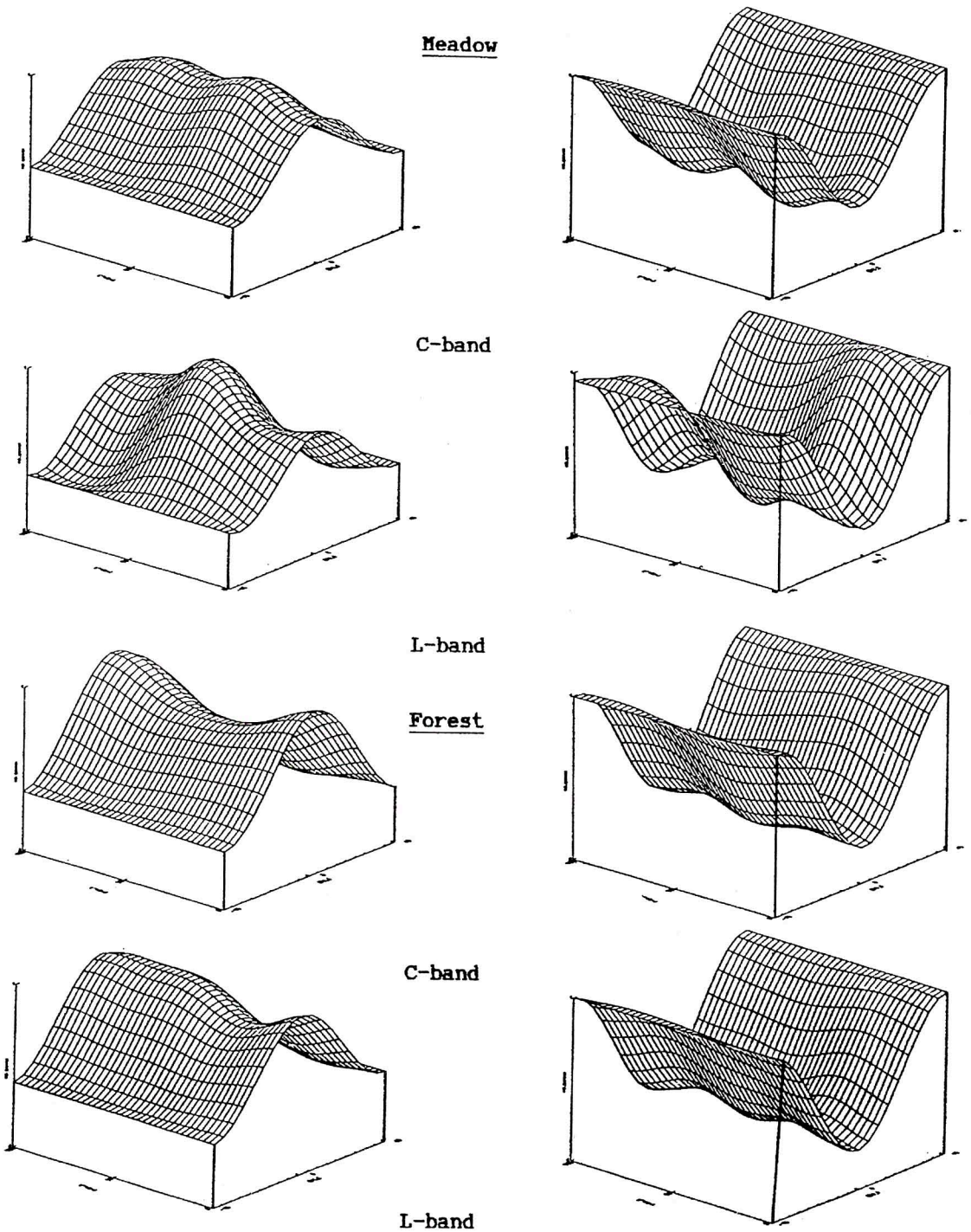

Fig. 5 - Polarization signatures (left: co-polarized, right: cross-polarized) of alpine meadows and alpine spruce forest of C- and L-band.

2.2 Heterogeinety of scatterers

Radar backscatter from an area consists of the superposition of a number of waves in a variety of polarizations. The polarization signature of a given pixel in a radar image represents the sum of many individual measurements. The polarization signatures of the individual measurements may not be identical. Hence their backscatter minima and maxima may occure at different polarizations if several scattering mechanisms are present.

The coefficient of variation (C.o.V.), defined as the ratio of the minimum power to the maximum power in a signature, indicates how much the signature components that make up the whole signature of an area vary. A small coefficient indicates that there are considerable differences between the minimum and maximum power, that the scattering mechanisms of the averaged pixels are relatively similar, or that the signal-to-noise ratio of the measurements is significant. Higher coefficients indicate that the scattering mechanisms within the averaged area vary or that the signal-to-noise ratio of the measurements is small. Tables 1, 2, 3 and 4 list the coefficients of variation from the studied sample matrices.

Tab. 1 - Coefficients of variation of the co-polarized signatures of C-band.

Surface Types	maximum			minimum			C.o.V.
	chi_t	psi_t	power	chi_t	psi_t	power	
Rock	0	5	1	40	85	0,0539	**0.0539**
Moraine	5	30	1	40	150	0,2324	**0.2324**
Meadow	0	60	1	-45	0	0,4266	**0.4266**
Forest	0	175	1	40	75	0,3143	**0.3143**

Tab. 2 - Coefficients of variation of the cross-polarized signatures of C-band.

Surface Types	maximum			minimum			C.o.V.
	chi_t	psi_t	power	chi_t	psi_t	power	
Rock	-45	0	1	0	5	0.0251	**0.0251**
Moraine	40	95	1	5	115	0.1742	**0.1742**
Meadow	-45	0	1	0	55	0.2594	**0.2594**
Forest	40	155	1	0	155	0.2164	**0.2164**

Tab. 3 - Coefficients of variation of the co-polarized signatures of L-band.

Surface Types	maximum			minimum			C.o.V.
	chi_t	psi_t	power	chi_t	psi_t	power	
Rock	-5	110	1	-35	35	0.0653	**0.0653**
Moraine	0	120	1	-40	35	0.2935	**0.2935**
Meadow	0	95	1	-35	150	0.2984	**0.2984**
Forest	0	160	1	-45	0	0.3927	**0.3927**

Tab. 4 - Coefficients of variation of the cross-polarized signatures of L-band.

Surface Types	maximum			minimum			C.o.V.
	chi_t	psi_t	power	chi_t	psi_t	power	
Rock	-40	45	1	-5	110	0.0653	**0.0653**
Moraine	-45	0	1	0	10	0.2304	**0.2304**
Meadow	-35	140	1	0	90	0.1656	**0.1650**
Forest	45	0	1	0	0	0.2385	**0.2385**

2.3 Polarization purity of received signal

In contrast to the transmitted signal, the signal received by the antenna is seldom completely polarized when observed as a function of time or spatial position. This is because the received signal, which represents the superposition of a large number of waves in a variety of polarizations, is the result of backscattering by a statistically random surface (Boerner *et* al. 1991). Knowledge of the Stokes parameters of the received signal allows the decomposition of a partially polarized return into unpolarized and fully polarized components:

$$\vec{S}^{rec} = (1 - m)\,\vec{S}_{un}^{rec} + m\,\vec{S}_{full}^{rec} \leftrightarrow \tag{8}$$

$$\begin{pmatrix} I_0 \\ Q \\ U \\ V \end{pmatrix} = (1 - m)\,I_0 \begin{pmatrix} 1 \\ 0 \\ 0 \\ 0 \end{pmatrix} + m\,I_0 \begin{pmatrix} 1 \\ \cos 2\chi \cos 2\psi \\ \cos 2\chi \sin 2\psi \\ \sin 2\chi \end{pmatrix} \tag{9}$$

where m is called "degree of polarization" and is defined as

$$m = \frac{polarized\ power}{total\ power} = \frac{\sqrt{Q^2 + U^2 + V^2}}{I_0} \tag{10}$$

Figures 6 and 7 display plots of the polarized and unpolarized components of the received signal as a function of the polarization state of the transmitted antenna from the test areas. As anticipated, surface cover types with a higher C.o.V. have more unpolarized power in the average received signal of all transmitted polarizations than areas with a low coefficient of variation. It can also be seen that the unpolarized signatures of such areas are similar in shape to the cross-polarized signatures for the same area. This implies that for areas with a higher C.o.V. the cross-polarized returns are mainly due to the unpolarized signal. For surface cover types with a low C.o.V., the unpolarized signatures are not the same as their cross-polarized signatures. This leads to the conclusion that the cross-polarized energy is not subject to unpolarized components in the backscatter, but rather to some polarization transformation associated with the actual scattering mechanism.

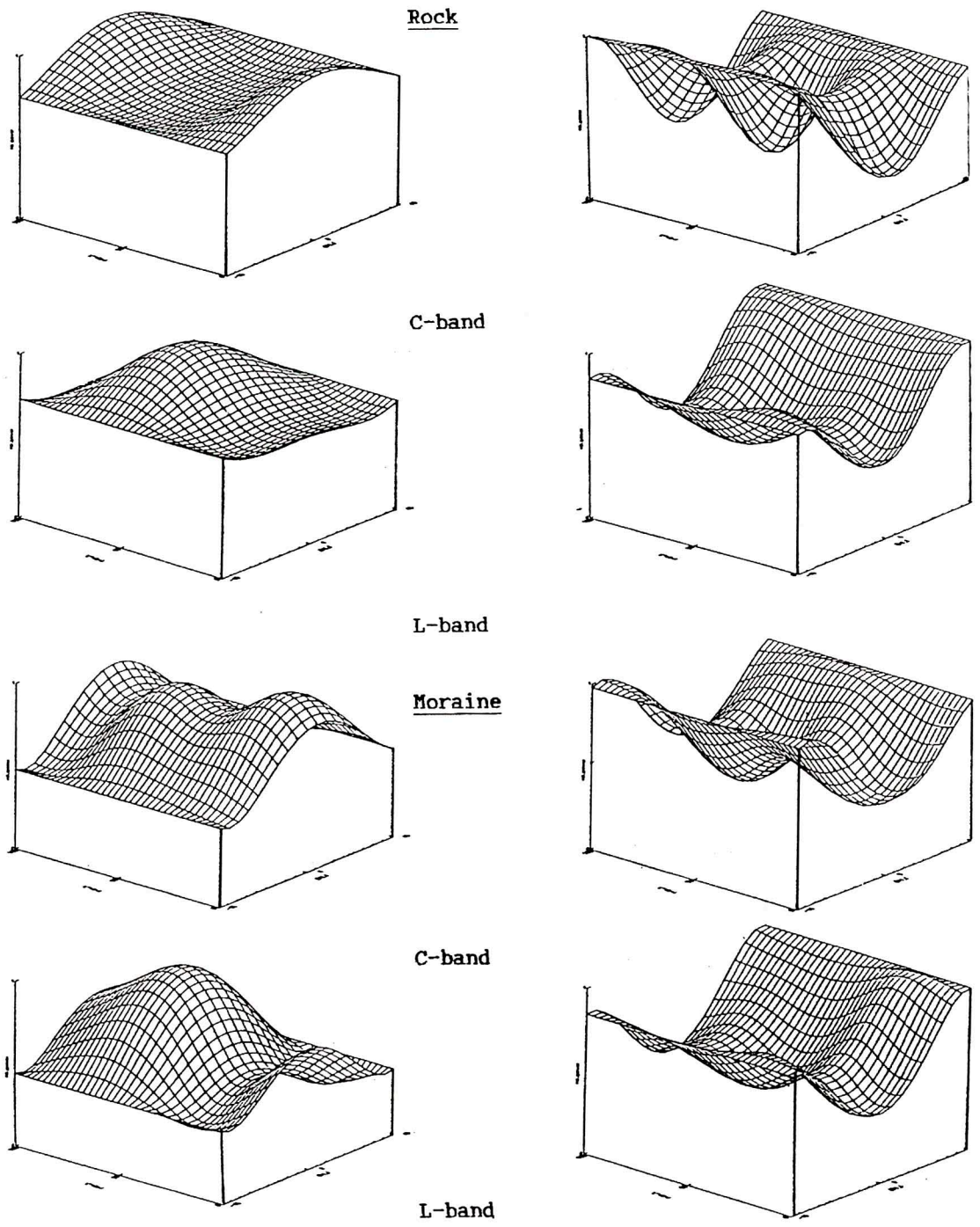

Fig. 6 - Polarized (left) and unpolarized (right) signatures of rock and moraine of C- and L-band.

The degree of polarization plotted as a function of the polarization state of the transmitted antenna is given in Figure 8. The signatures do not represent absolute values but normalized ones. They are an indicator for the purity of the radar signal. However, only their extreme values are significant.

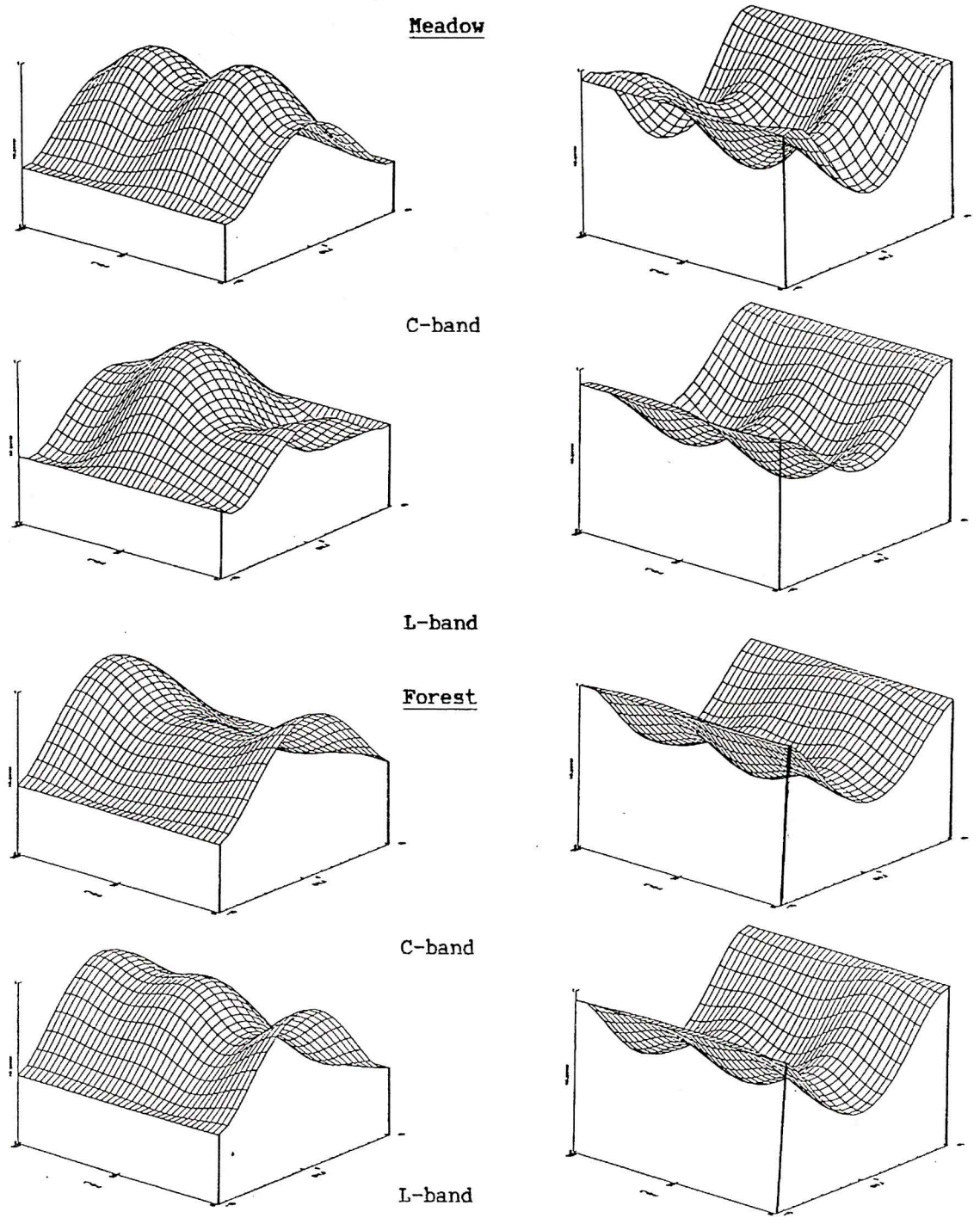

Fig. 7 - Polarized (left) and unpolarized (right) signatures of alpine meadows and alpine spruce forest of C- and L-band.

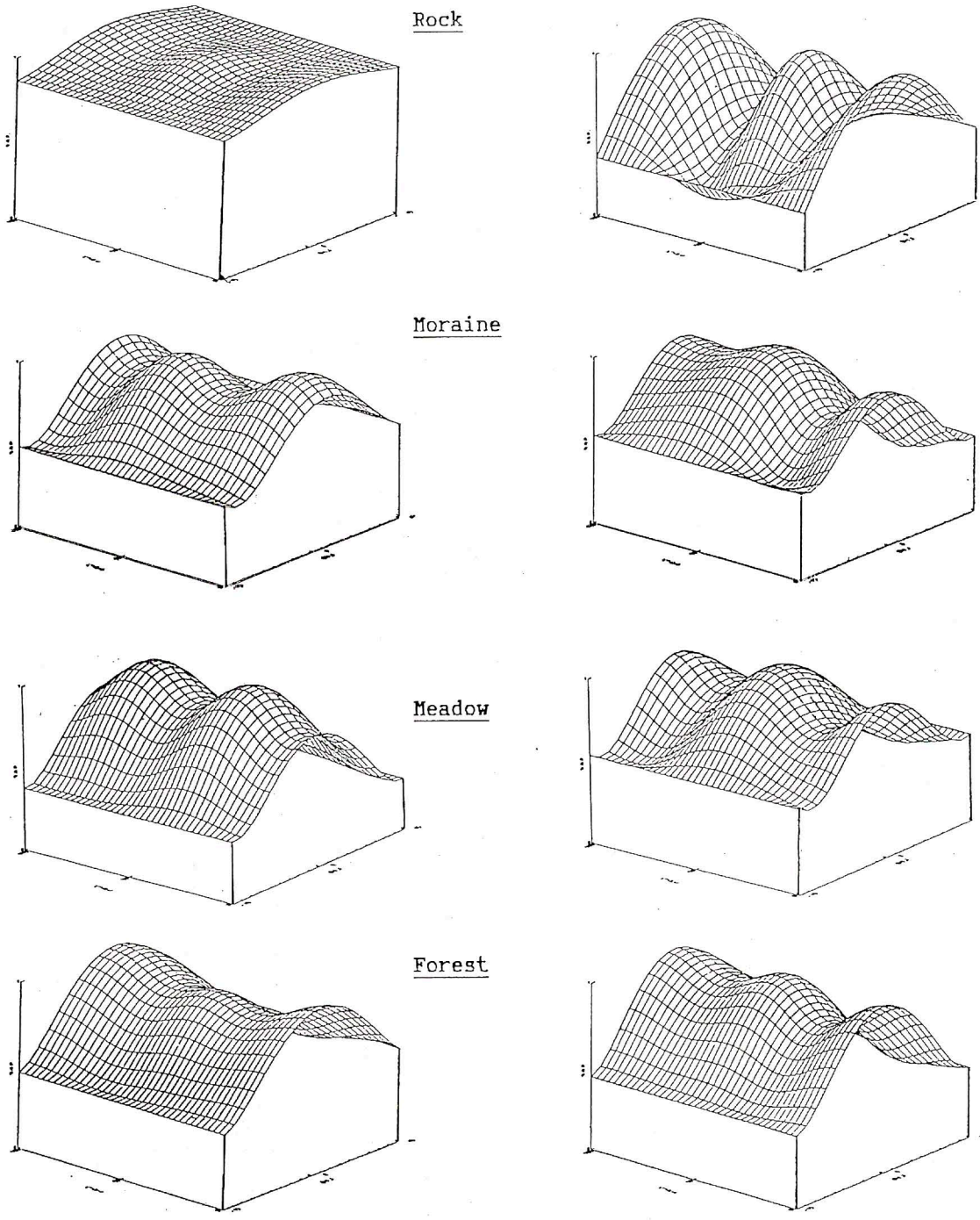

Fig. 8 - Degree of polarization signatures of the surface cover types studied a) rock b) moraine c) meadow d) forest (left: C-band, right: L-band).

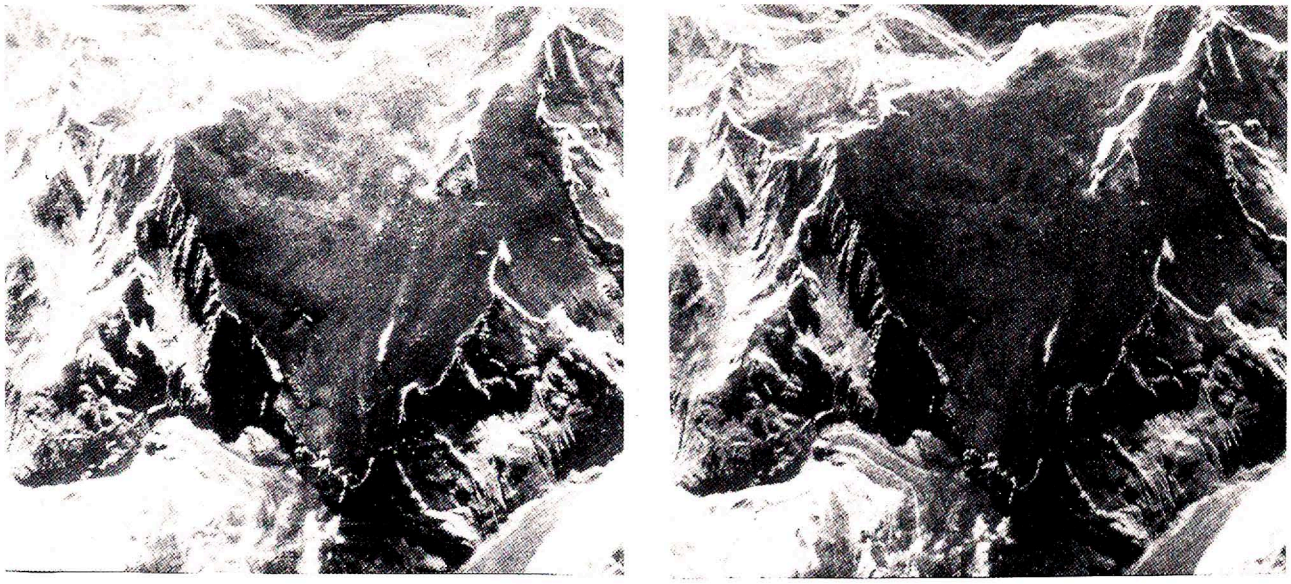

Fig. 9 - Images generated to maximize (left) and minimize returns (right) from the moraine class for an optimal depiction of this surface type. Note that the gray value distribution is only subject to optimized polarizations parameters. No further manipulations have bean applied.

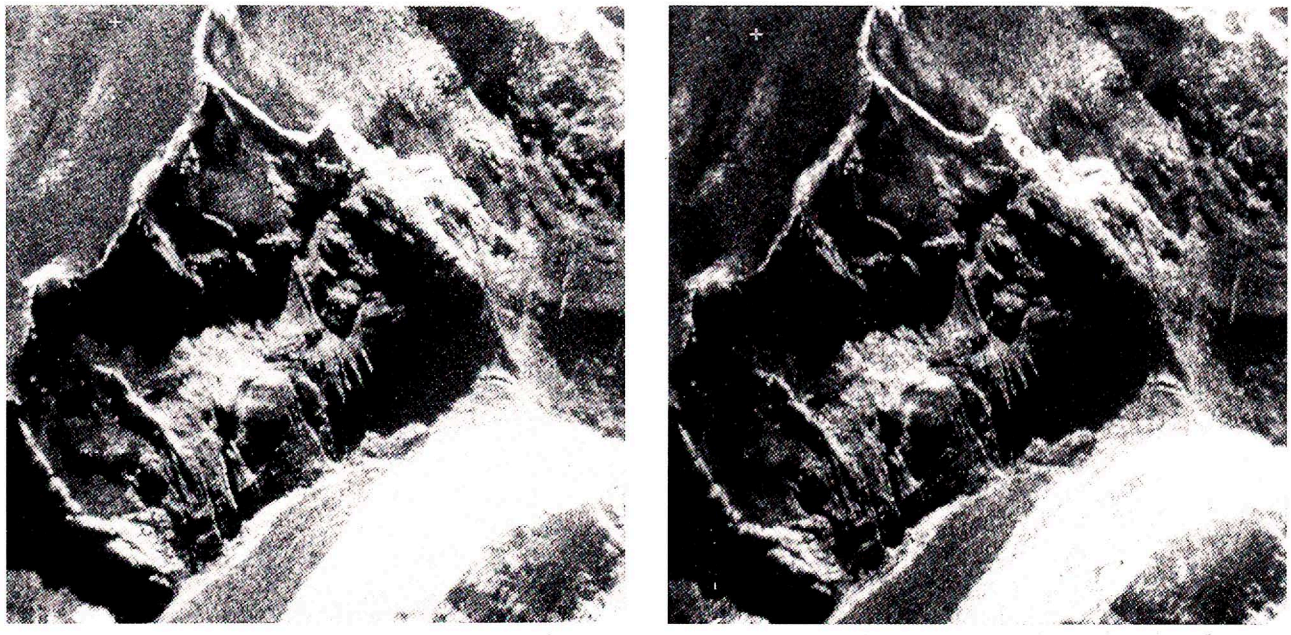

Fig. 10 - Images generated to maximize (left) and to minimize returns (right) from the rock class for an optimal depiction of this surface type. Note that the gray value distribution is only subject to optimized polarizations parameters. No further manipulations have bean applied.

2.4 Polarization optimization

The capability to separate a composite signature into its components enables us to generate images that maximize and minimize the polarized or unpolarized returns from particular surfacecover types (Evans *et al.* 1988). This process is called polarization filtering (Boerner 1981), (Kostinski it *et al.* 1988). Optimal polarization images may be generated, either by 1) maximizing the backscatter return by choosing a transmitted polarization that maximizes the average power of the scattered waves or by 2) minimizing the backscatter return by choosing a transmitted polarization that minimizes the average power of the scattered waves. The polarization of the receiving antenna is calculated on a pixel-by-pixel basis to either maximize or minimize the backscatter of each pixel.

For areas with a low coefficient of variation the images which were generated with the parameters for the maximum and minimum power show the biggest differences, while areas with a high coefficient of variation for images generated in a similar way show very little changes. Figures 9 and 10 show images generated with optimized polarization parameters.

2.5 Contrast enhancement

In this chapter a method to find the optimum polarization in order to enhance the contrast between two types of scatterers is described. The polarization of the receive and transmit antennas which maximizes the ratio of the signal power scattered by one type of scatterer (called "target") to that scattered by another type of scatterer (called "clutter") has to be found (Shi, Dozier, Rott and Davis 1991). In other words we will find the maxima of

$$C\,R\,(\chi_t, \psi_t, \chi_r, \psi_r) = \frac{P_{target}\,(\chi_t, \psi_t, \chi_r, \psi_r)}{P_{clutter}\,(\chi_t, \psi_t, \chi_r, \psi_r)} = \frac{\vec{S}(\psi_r, \chi_r)\,[M]_{target}\,\vec{S}(\psi_t, \chi_t)}{\vec{S}(\psi_r, \chi_r)\,[M]_{clutter}\,\vec{S}(\psi_t, \chi_t)} \tag{11}$$

where ψ_t, χ_t and ψ_r, χ_r refer to the polarization of the transmitting and receiving antennas, have to be determined. For a fixed transmitting polarization, the maximum and minimum contrast ratios are given by

$$C\,R_{max}\,(\psi_t, \chi_t) = \frac{S_{01}\,S_{02} - s_1\,s_2}{S_{02}^2 - s_2\,s_2} + \sqrt{\left(\frac{S_{01}\,S_{02} - s_1\,s_2}{S_{02}^2 - s_2\,s_2}\right)^2 - \frac{S_{01}^2 - s_1\,s_1}{S_{02}^2 - s_2\,s_2}} \tag{12}$$

$$C\,R_{min}\,(\psi_t, \chi_t) = \frac{S_{01}\,S_{02} - s_1\,s_2}{S_{02}^2 - s_2\,s_2} + \sqrt{\left(\frac{S_{01}\,S_{02} - s_1\,s_2}{S_{02}^2 - s_2\,s_2}\right)^2 - \frac{S_{01}^2 - s_1\,s_1}{S_{02}^2 - s_2\,s_2}} \tag{13}$$

where

$$\begin{pmatrix} S_{01} \\ s_1 \end{pmatrix} = [M]_1\,\vec{S}(\psi_t, \chi_t)\,,\ \begin{pmatrix} S_{02} \\ s_1 \end{pmatrix} = [M]_2\,\vec{S}(\psi_t, \chi_t) \tag{14}$$

$\vec{S}(\psi_t, \chi_t)$ being the Stokes vector of the transmitting antenna.

The optimum contrast ratios are only functions of the transmitting antenna polarization. Signatures in which the contrast ratio is plotted as a function of the transmitting antenna polarization are called contrast ratio signatures. The optimum transmitting polarization can be numerically derived from the above equations. Once the maximum contrast is found, the optimum receiving polarization can be calculated by

$$a_r = \frac{s\,(C\,R_{opt})}{\sqrt{s\,(C\,R_{opt}\,s\,(C\,R_{opt})}} \tag{15}$$

where

$$s\,(C\,R_{opt}) = s_1 - C\,R_{opt}\,s_2 \tag{16}$$

and $C\,R_{opt}$ is the maximum of $C\,R_{max}$, optimized over all transmitting antenna polarizations. The selection of the optimum polarization to enhance the contrast between two types of scatterers can be intepreted as a polarization filter. The filter parameters are those that yield the maximum of the contrast ratio signatures.

The performance of the filter is related to the dependence of the contrast ratio from the polarization in the nearness of the maximum. If the contrast ratio varies strongly as a function of polarization we have a significant decrease in the filter performance for a small deviation in antenna polarization.

The enhancement factor *EF*, a quantity for the performance of the polarization filter, is defined as

$$EF = \frac{\vec{S}(\psi_r, \chi_r)\,[M]_{target}\,\vec{S}(\psi_t, \chi_t)\,(M_{11})_{clutter}}{\vec{S}(\psi_r, \chi_r)\,[M]_{clutter}\,\vec{S}(\psi_t, \chi_t)\,(M_{11})_{target}} \tag{17}$$

Tables 5 and 6 list the filter parameters and theenhancement factor from the studied sample matrices.

Tab. 5 - Polarization filtering parameters and enhancement factor (C-band).

Surface Contrast	Transmitter		Reveiver		EF in dB
	chi_t	psi_t	chi_r	psi_r	
Forest-Moraine	10	25	-43,8	-0,6	**1.7135**
Meadow-Forest	5	35	-44,4	-0,1	**1.2919**
Meadow-Moraine	-5	110	-43,8	-0,3	**2.0998**
Rock-Moraine	-25	140	-44,7	-0,8	**1.5101**
Rock-Meadow	35	175	-44,7	0,1	**1.6021**
Rock-Forest	-35	30	-44,8	0,5	**1.3784**

Tab. 6 - Polarization filtering parameters and enhancement factor (L-band).

Surface Contrast	Transmitter		Reveiver		EF in dB
	chi_t	psi_t	chi_r	psi_r	
Forest-Moraine	-25	80	-43,9	0,6	**1.3512**
Meadow-Forest	0	170	-43,9	-0,6	**1.5106**
Meadow-Moraine	-30	120	-43,5	-0,7	**1.6619**
Rock-Moraine	35	125	-44,5	-0,7	**1.5015**
Rock-Meadow	15	145	-44,2	0,8	**1.9958**
Rock-Forest	20	125	-44,5	0,6	**1.5972**

CONCLUSION

In this paper techniques to analyse polarization signatures of natural surfaces in high-alpine environments are presented. The investigations show that the shape of the polarimetric signatures and the associated pedestal is characteristic for each surface class. This allows the generation of optimized images for each class, and in the future a more precise classification of surface types. The contrast enhancement results give the possibility to generate optimized images, a first step towards thematic mapping in complex alpine terrains. This indicates the high potential of multifrequency polarimetric SAR data for geo-applications in alpine environments. Ongoing research activities at the author's institute, based on Fourier analysis, may still lead further in this direction.

ACKNOWLEDGMENTS

The authors would like to thank Dr. H. Rott (Institute for Meteorology and Geophysics of the University of Innsbruck) for data provision and many constructive comments, which significantly contributed to the results presented in this paper. Special thanks go to the radar group of the authors' Institute for Image Processing and Computer Graphics for their assistance.

REFERENCES

Agrawal A.P. and Boerner W-M., 1991, "Description of A Monostatic Polarimetric Radar Model for Fluctuating Distributed Scatterers with Applications to Rain Backscatter", Math. and Phys. Science, Vol. C-350, Part 2, pp 1779-1806.

Boerner W-M., 1981, "Use of Polarization Depence in Electromagnetic Inverse Scattering", Radio Science, Vol. 16, pp 1037-1045.

Boerner W-M., Yan W-L., Yamaguchi Xi and Y., 1991, "On the Basic Principles of Radar Polarimetry: The Target Characteristic Polarization State Theory of Kennaugh, Huynen's Polarization Fork Concept, and Its Extension to the Partially Polarized Case", IEEE Proceedings, Vol. 79, No.10, pp 1538- 1550.

Boerner W-M., Liu C-L., Zhang X., 1992, "Comparison of Optimization Procedures for 2x2 Sinclair, 3x3 Covariance, and 4x4 Mueller/Kennaugh (symmetric) Matrices in Coherent Radar Polarimetry and its Applications to Target versus Backround Clutter Discrimination in Microwave Sensing and Imaging", Int'l. Journal on Advances in Remote Sensing, Vol.2, No4.

Dubois P.C. and Norikane L., 1987, "Data Volume Reduction For Imaging Radar Polarimetrie", Proceedings of IGARSS '87 Symposium, pp 691-696.

Evans D.L., Farr T.G., van Zyl J.J. and Zebker H.A., 1988, "Radar Polarimetrie: Analysis Tools and Applications", IEEE Transactions on Geoscience and Remote Sensing, vol. 26, pp 774-789.

Jiancheng Shi, Dozier J., Rott H., and Davis R.E., 1991, "Snow and Glacier Mapping in Alpine Regions With Polarimetric SAR", IGARSS '91: Remote Sensing: Global Monitoring for Earth Management, vol. 4, pp 2312-2314.

Reck M. and Schreier G., 1990, "Fourier Series Representation of SAR Polarimetric Scattering Signatures", IGARSS '91: Remote Sensing: Science for the Nineties, vol. 2, pp 1687-1690.

Rott H., 1991, "Multi-Parameter SAR Experiments on Snow and Glacier Applications", EARSeL Symposium 1991.

Ulaby F.T., Elachi T. and editors, 1990, "Radar Polarimetry for Geoscience Applications", Artech House.

van Zyl J.J., Zebker H.A. and Elachi C., 1987, "Imaging Radar Polarization Signatures: Theory and Observation", Radio Science, vol.22, Number 4, pp 529-543.

Zebker H.A.,van Zyl J.J. and Held D.N., 1987, "Imaging Radar Polarimetry From Wave Synthesis", Journal of Geophisical Research, vol.92, B1, pp 683-701.

Zebker H.A., and Yunling Lou, 1990, "Phase Calibration of Imaging Radar Polarimeter Stokes Matrices", IEEE Transactions on Geoscience and Remote Sensing, vol. 28, pp 246-252.